MBoC | BRIEF REPORT

The GTP-tubulin cap is not the determinant of microtubule end stability in cells

Anna Cassidy[a,†], Veronica Farmer[a,b,†], Göker Arpağ[a,c], and Marija Zanic[a,d,e,*]

[a]Department of Cell and Developmental Biology, Vanderbilt University, Nashville, TN 37205; [b]Department of Cell Biology, Duke University School of Medicine, Durham, NC 27710; [c]Department of Molecular Biology and Genetics, Kadir Has University, Istanbul, Turkey 34083; [d]Department of Chemical and Biomolecular Engineering, Vanderbilt University, Nashville, TN 37235; [e]Department of Biochemistry, Vanderbilt University, Nashville, TN 37205

ABSTRACT **Microtubules are dynamic cytoskeletal polymers essential for cell division, motility, and intracellular transport. Microtubule dynamics are characterized by dynamic instability—the ability of individual microtubules to switch between phases of growth and shrinkage. Dynamic instability can be explained by the GTP-cap model, suggesting that a "cap" of GTP-tubulin subunits at the growing microtubule end has a stabilizing effect, protecting against microtubule catastrophe—the switch from growth to shrinkage. Although the GTP-cap is thought to protect the growing microtubule end, whether the GTP-cap size affects microtubule stability in cells is not known. Notably, microtubule end-binding proteins, EBs, recognize the nucleotide state of tubulin and display comet-like localization at growing microtubule ends, which can be used as a proxy for the GTP-cap. Here, we employ high spatiotemporal resolution imaging to compare the relationship between EB comet size and microtubule dynamics in interphase LLC-PK1 cells to that measured in vitro. Our data reveal that the GTP-cap size in cells scales with the microtubule growth rate in the same way as in vitro. However, we find that microtubule ends in cells can withstand transition to catastrophe even after the EB comet is lost. Thus, our findings suggest that the presence of the GTP-cap is not the determinant of microtubule end stability in cells.**

SIGNIFICANCE STATEMENT

- The cap of GTP-tubulin has been established as the main stabilizing feature at growing microtubule ends; however, recent studies using biochemical in vitro reconstitution have questioned what aspects of the GTP-cap define microtubule end stability.
- By comparing EB comets on microtubule ends in cells and in vitro using high spatiotemporal resolution imaging, the authors find that the GTP-tubulin cap is not the determinant of microtubule end stability in cells.
- These results shed light on the molecular mechanisms regulating microtubule dynamics in living cells.

Monitoring Editor
Alexander Mogilner
New York University

Received: Jul 18, 2024
Revised: Aug 26, 2024
Accepted: Aug 26, 2024

Cross-Validation

New Methods

INTRODUCTION

Microtubules are dynamic cytoskeletal polymers essential for cellular processes including cell division, intracellular transport, and cell motility (Alberts *et al.*, 2002). For microtubules to accomplish such diverse cellular functions, the architecture of the microtubule network needs to remodel in space and time. This dynamic remodeling is facilitated by the regulation of dynamics of individual microtubule polymers, which switch between phases of growth and shrinkage through a process known as "microtubule dynamic instability" (Mitchison and Kirschner, 1984; Kirschner and Mitchison, 1986). Dynamic instability is powered by the GTPase activity of tubulin. Namely, microtubule polymers grow via addition of GTP-bound $\alpha\beta$-tubulin heterodimers to the growing end (Caplow and Reid, 1985). Following dimer addition, GTP in the β-tubulin subunit is hydrolyzed (Carlier and Pantaloni, 1982; Nogales *et al.*, 1998), leading to a conformational change in the tubulin dimer that ultimately results in an inherently unstable GDP-tubulin lattice (Alushin *et al.*, 2014; Manka and Moores, 2018b; Zhang *et al.*, 2018; Estévez-Gallego *et al.*, 2020; Gudimchuk and McIntosh, 2021). However, the delay in GTP-hydrolysis following dimer addition results in a region of GTP-tubulin at the growing microtubule end, aptly termed the "GTP-cap" (Mitchison and Kirschner, 1984). The length of this GTP-tubulin region is dependent on two factors: 1) the rate of GTP-tubulin addition (microtubule polymerization rate) and 2) the rate of tubulin GTP-hydrolysis within the polymer. The GTP-cap provides a stabilizing structure at the end of the growing microtubule, and its loss is thought to trigger microtubule catastrophe, the transition of the microtubule end from a growing to a shrinking state (Kirschner and Mitchison, 1986; Drechsel and Kirschner, 1994; Caplow and Shanks, 1996).

Investigation of the spatiotemporal properties of the GTP-cap has been facilitated by the discovery that microtubule tip-tracking proteins from the EB family are sensitive to the nucleotide state of tubulin and preferentially associate with the GTP-cap at growing microtubule ends (Zanic *et al.*, 2009; Maurer *et al.*, 2012; Zhang *et al.*, 2015; Roostalu *et al.*, 2020). Both in cells and in vitro, EBs display a characteristic comet-like localization at growing microtubule ends, consistent with the decay of the GTP-cap due to GTP-hydrolysis (Mimori-Kiyosue *et al.*, 2000; Tirnauer *et al.*, 2002; Bieling *et al.*, 2007; Dixit *et al.*, 2009). Measurements of EB comets have allowed investigation of the relationship between GTP-cap size, microtubule growth rate, and microtubule stability using purified proteins in vitro. Recent studies have established that EB comet size scales linearly with the microtubule growth rate, irrespective of whether increasing growth rates are accomplished using increasing concentrations of tubulin or by addition of regulatory proteins (Bieling *et al.*, 2007; Dixit *et al.*, 2009; Farmer *et al.*, 2021). Interestingly, however, it was found that the mean size of the GTP-cap does not reflect overall microtubule stability. Although larger GTP-caps correlate with suppression of microtubule catastrophe for microtubules grown with tubulin alone (Duellberg *et al.*, 2016; Roostalu *et al.*, 2020; Farmer *et al.*, 2021), this relationship can be disrupted by the effects of regulatory proteins. For example, acceleration of microtubule growth by microtubule polymerase XMAP215 resulted in a simultaneous increase of the EB comet length and the frequency of microtubule catastrophe (Farmer *et al.*, 2021). Thus, the size of the GTP-cap alone cannot predict microtubule end stability in vitro.

In cells, microtubule dynamics are regulated by myriad microtubule-associated proteins (MAPs). Findings that the addition of even a single MAP in vitro can alter the relationship between GTP-cap size and microtubule stability motivates the investigation of these relationships in a cellular context, where MAPs are abundant. Recent studies revealed that GTP-cap size also increases with microtubule growth rate in cells (Urazbaev *et al.*, 2021). However, it is unclear whether the relationship between growth rate and GTP-cap size in cells is the same as in vitro. Furthermore, the role of the GTP-cap in defining microtubule end stability in cells is not known. Here, we use high spatiotemporal resolution imaging of EB comets in vitro and in interphase LLC-PK1 cells to elucidate the relationship between the GTP-cap and microtubule end stability in cells.

RESULTS

The size of EB comets in vitro and in cells can be directly compared using fast super-resolution microscopy

To compare the size of the GTP-cap in vitro to that in cells, we measured the lengths of EB1-GFP comets in both systems (Figure 1A). To achieve the most accurate comparison, we sought to image the two systems with high spatiotemporal resolution using the same imaging modality. In vitro reconstitution assays of microtubule dynamics typically use total internal reflection fluorescence (TIRF) microscopy (Gell *et al.*, 2010; Zanic, 2016). These assays are inherently two-dimensional, making TIRF an ideal imaging modality, as it illuminates only an ~100 nm slice of the sample directly above the cover glass. However, TIRF microscopy does not permit imaging of microtubules deeper into the cell. We thus opted to use Instant Structured Illumination Microscopy (iSIM)—a fast super-resolution fluorescence imaging technique that provides both a high signal-to-noise ratio in our in vitro assay and imaging into the z-plane of the cell (York *et al.*, 2013; Roth and Heintzmann, 2016). In contrast to traditional SIM, which requires computational postprocessing to generate a super-resolution image, iSIM creates a super-resolution analog image in real time using a series of microlenses and galvo-scanning mirrors (York *et al.*, 2013; Curd *et al.*, 2015). Indeed, we found that iSIM enabled imaging of EB1-GFP comets at the ends of growing microtubules both in vitro and in cells with high spatiotemporal resolution (Figure 1, B and C).

To image EB comets in our in vitro reconstitution system, dynamic microtubule extensions were polymerized from GMPCPP-stabilized seeds in the presence of EB1-GFP, as described previously (Zanic *et al.*, 2009; Farmer *et al.*, 2021). For cellular imaging of EB comets, we used porcine kidney epithelial cells (LLC-PK1) stably expressing EB1-GFP, an established model for imaging microtubule dynamics (Rusan *et al.*, 2001; Piehl and Cassimeris, 2003). In addition to using the same imaging modality, we matched the imaging conditions, including laser power, exposure time, imaging interval, and temperature (see *Materials and Methods*).

This article was published online ahead of print in MBoC in Press (http://www.molbiolcell.org/cgi/doi/10.1091/mbc.E24-07-0307).

Author contributions: A.C., V.F., and M.Z. conceived and designed the experiments; A.C. and V.F. performed the experiments; A.C., V.F., and G.A. analyzed the data; A.C., V.F., and M.Z. drafted the article; A.C. and V.F. prepared the digital images; M.Z. supervision, funding, writing.

Conflicts of interest: The authors declare no financial conflict of interest.

†These authors contributed equally as co-first authors to this work.

*Address correspondence to: Marija Zanic (marija.zanic@vanderbilt.edu).

Abbreviations used: CLASP, cytoplasmic linker associated protein; MAP, microtubule associated protein; SDC, spinning disk confocal; SEM, standard error of the mean; TIRF, total internal reflection fluorescence microscopy.

© 2024 Cassidy *et al.* This article is distributed by The American Society for Cell Biology under license from the author(s). It is available to the public under an Attribution 4.0 International Creative Commons CC-BY 4.0 License (https://creativecommons.org/licenses/by/4.0/).

"ASCB®," "The American Society for Cell Biology®," and "Molecular Biology of the Cell®" are registered trademarks of The American Society for Cell Biology.

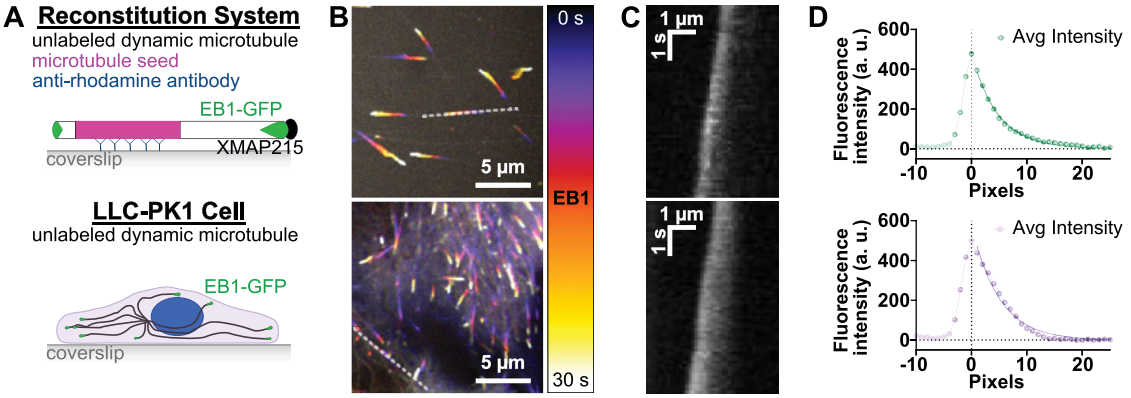

FIGURE 1: The size of the EB comets in vitro and in cells can be directly compared using fast super-resolution microscopy. (A) Schematic of in vitro reconstitution and cellular assays used to image EB comets. Top, unlabeled tubulin was polymerized from GMPCPP-stabilized rhodamine microtubule seeds in the presence of EB1-GFP. Bottom, LLC-PK1 cells stably overexpressing EB1-GFP. (B) EB1-GFP imaged using iSIM in vitro (top) and in cells (bottom). EB1-GFP location was temporally color-coded over 30 s of imaging. (C) Kymographs representing individual EB1-GFP comets over time, as indicated by white dotted lines in B. (D) The averaged EB1-GFP comet profiles were fit to an exponential decay to determine the average comet lengths.

Furthermore, the subsequent image analysis pipeline was identical between the two systems (Supplemental Figure S1). The EB1-GFP comet intensity profiles were fit to an exponential decay function, and the decay constant was used as a proxy for the comet size (Figure 1D). Using this approach, we could directly compare the sizes of EB comets on microtubules grown in vitro to those in cells.

The scaling between EB comet length and microtubule growth rate in cells is the same as in vitro

To directly compare the relationship between microtubule growth rate and GTP-cap size in cells and in vitro, we measured the EB comet size at growing microtubule ends in both systems over a range of microtubule growth rates. First, we confirmed that the inherent variability in EB1-GFP expression levels in the stably-expressing LLC-PK1 cells does not significantly impact microtubule dynamics (Supplemental Figure S2), consistent with previous reports (Piehl and Cassimeris, 2003). Overall, microtubules growing in LLC-PK1 cells displayed growth rates up to ~230 nm/s (Figure 2; Supplemental Figure S2). These fast cellular growth rates can be achieved in vitro through synergistic effects of the microtubule polymerase XMAP215 with EB1 (Zanic *et al.*, 2013; Farmer *et al.*, 2021). In our in vitro assay, we sought to employ our purified protein components at concentrations consistent with those measured in cells (Hiller and Weber, 1978; Tournebize *et al.*, 2000; Tirnauer *et al.*, 2002; Juanes *et al.*, 2020). Specifically, we found that a combination of 12 µM tubulin, 100 nM XMAP215, and 200 nM EB1-GFP resulted in microtubules polymerizing over a comparable range of growth rates to those observed in LLC-PK1 cells. Each growth event was defined by a 5-s (65 frame) period of growth and the growth rate was determined using linear regression of displacement over time (see *Materials and Methods*; Supplemental Figure S1). EB1-GFP comet sizes increased linearly with microtubule growth rate in vitro (Figure 2A), as reported previously (Bieling *et al.*, 2007; Farmer *et al.*, 2021). We observed that the size of EB1-GFP comets in cells also increased linearly with microtubule growth

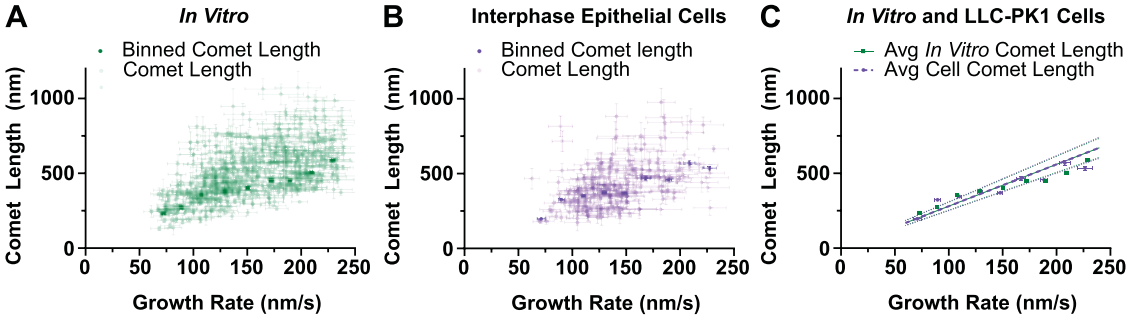

FIGURE 2: The scaling between the EB comet length and the microtubule growth rate in cells is the same as in vitro. (A) Microtubule growth events polymerized using 12 µM unlabeled tubulin, 200 nM EB1-GFP, and 100 nM XMAP215. Each dot represents the mean growth rate and EB1 comet size along a 5-s-long growth event ± 95% CI, $N = 471$ growth events. Individual events were binned into 20 nm/s bins. Bold dots represent weighted averages with weighted errors of 95% CI for each bin. (B) Microtubule growth events from LLC-PK1 cells stably overexpressing EB1-GFP. Each dot represents the mean growth rate and EB1 comet size along a 5-s-long growth event ± 95% CI, $N = 178$ growth events from 16 cells. Individual events were binned into 20 nm/s bins. Bold dots represent weighted averages with weighted errors of 95% CI for each bin. (C) The binned weighted average growth rates and comet sizes per condition were fit to a linear regression. 95% CI shown by the dotted lines. Three biological replicates were performed for each condition.

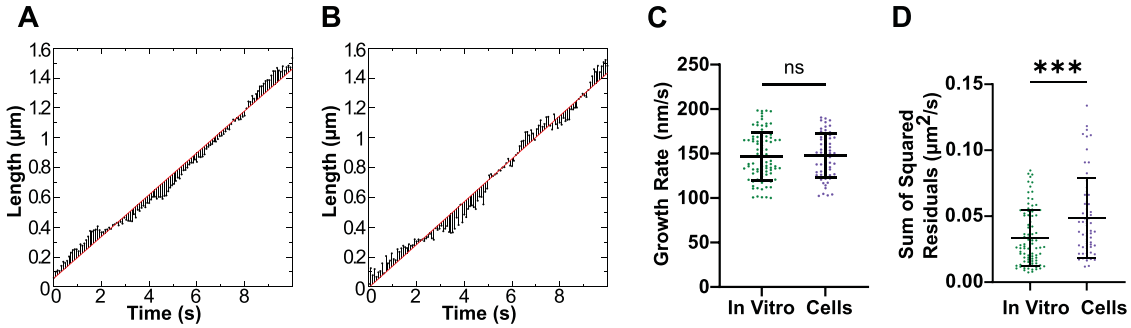

FIGURE 3: Microtubules in cells display larger growth-rate fluctuations than in vitro. (A and B) Growth rate–matching conditions achieved by either (A) 12 μM tubulin, 200 nM EB1-GFP, and 100 nM XMAP215 in vitro or (B) expressing EB1-GFP in interphase LLC-PK1 cells. Representative tracks showing microtubule tip position (black points), residuals for each timepoint (black lines), and linear regression of tip position (red line). (C) Growth rate for each segment; in vitro, 150 ± 30 nm/s (mean ± SD, $n = 88$); in cells, 150 ± 20 nm/s (mean ± SD, $n = 62$). $p > 0.9$, unpaired Student's t test. (D) SSR for each 10 s segment; in vitro, 0.034 ± 0.021 μm^2/s (mean ± SD, $n = 88$); in cells, 0.049 ± 0.030 μm^2/s (mean ± SD, $n = 62$). $p = 0.001$, Mann–Whitney U test.

rate (Figure 2B). Strikingly, fitting the data to a linear regression curve revealed that the relationship between the EB comet size and the microtubule growth rate is the same in two systems (Figure 2C, slope of 2.79 s [95% confidence interval, CI: 2.53 s–3.06 s] in vitro vs. 2.79 s [95% CI: 2.50 s–3.09 s] in cells). This observation suggests that microtubule growth rate is the primary determinant of EB1-GFP comet size both in vitro and in interphase epithelial cells.

In general, the size of the EB comet is set by the balance of microtubule growth, which adds new GTP-tubulin subunits to the growing microtubule end, and GTP-hydrolysis, which ultimately transforms tubulin subunits into a GDP-bound state not recognized by EB. Our finding that the scaling between the EB1-GFP comet size and the microtubule growth rate is identical in interphase LLC-PK1 cells to that observed in vitro suggests that the GTP-hydrolysis rate is not directly and differentially regulated in this cellular system. Indeed, our measurements are consistent with a single, comparable hydrolysis rate both in vitro and in LLC-PK1 cells. The determined slopes of the relationship between the comet size and microtubule growth yield a hydrolysis rate of ~0.4 s^{-1}, consistent with the rates previously estimated both in and outside of cells (Seetapun *et al.*, 2012; Maurer *et al.*, 2014; Roostalu *et al.*, 2020). Thus, our results suggest that changing the size of the GTP-cap through modulation of the GTP-hydrolysis rate is not a mechanism employed by interphase cells to regulate microtubule dynamics. Furthermore, the finding that the scaling between the EB1-GFP comets and the microtubule growth rate observed in vitro is the same in interphase LLC-PK1 cells validates the use of our in vitro reconstitution assay to interrogate the role of the GTP-cap in microtubule end stability and the overall molecular mechanisms of microtubule dynamics.

Microtubules in cells display larger growth-rate fluctuations than in vitro

Our investigation of the relationship between EB comet size and the microtubule growth rate relied on our ability to determine the microtubule growth rate with high accuracy. To achieve this, we opted to measure EB1-GFP comets over short (5-s/65 frame), linear growth intervals. Even over such short time intervals, and although we used identical imaging conditions, the proportion of growth events that were not well fit by linear regression was significantly larger in cells than in vitro (Supplemental Figure S1, 61% in cells vs. 38% in vitro, using $R^2 < 0.8$ criterium). This observation suggests that microtubule tips in cells undergo significant growth rate fluctuations. To investigate deviations from the mean microtubule growth rate further, we compared two groups of growth events displaying matching mean growth rates over longer, 10-s periods of growth (Figure 3, A–C). We used the sum of squared residuals (SSR) as a measure of the deviation from the linear regression growth rate for each growth event. We found that SSR was significantly higher in cells (0.049 ± 0.030 μm^2/s, mean ± SD, $n = 62$) than in vitro (0.034 ± 0.021 μm^2/s, mean ± SD, $n = 88$; $p = 0.001$, Mann–Whitney U test; Figure 3D). This result demonstrated that growing microtubules in cells indeed display a higher degree of growth rate variability than those polymerized at the same mean growth rates in vitro.

Previous studies in vitro suggested that fluctuations in growth rate are accompanied by morphological changes at the growing microtubule end, which can ultimately destabilize the end structure and result in the onset of microtubule catastrophe (Coombes *et al.*, 2013; Farmer *et al.*, 2021; Farmer and Zanic, 2022). Interestingly, CLASP proteins allow microtubules to withstand a larger degree of growth fluctuations by stabilizing an intermediate pre-catastrophe state of the microtubule end (Aher *et al.*, 2018, 2020; Lawrence *et al.*, 2018, 2020, 2023; Lawrence and Zanic, 2019; Mahserejian *et al.*, 2022). Notably, although the microtubules in cells displayed a large degree of growth rate variability, we did not observe aberrant EB comet morphologies or visibly tapered microtubule end structures previously seen in vitro (Coombes *et al.*, 2013; Aher *et al.*, 2018; Reid *et al.*, 2019; Farmer *et al.*, 2021; Gudimchuk and McIntosh, 2021). This suggests that CLASPs, as well as potentially other MAPs present at the microtubule ends, promote microtubule end repair and stability, despite large growth-rate fluctuations observed in cells.

EB localization does not predict microtubule catastrophe in cells

Microtubules growing from purified tubulin in vitro display a stereotypical slowdown and loss of EB comet prior to the onset of catastrophe (Maurer *et al.*, 2012; Farmer *et al.*, 2021). Whether a similar slowdown in growth rate and decay of the EB comet predicts the onset of catastrophe in cells is not known. To investigate this, we sought to image EB localization at high spatiotemporal resolution over the course of microtubule catastrophe (see *Materials and Methods*). Because EB proteins track growing, but not shrinking

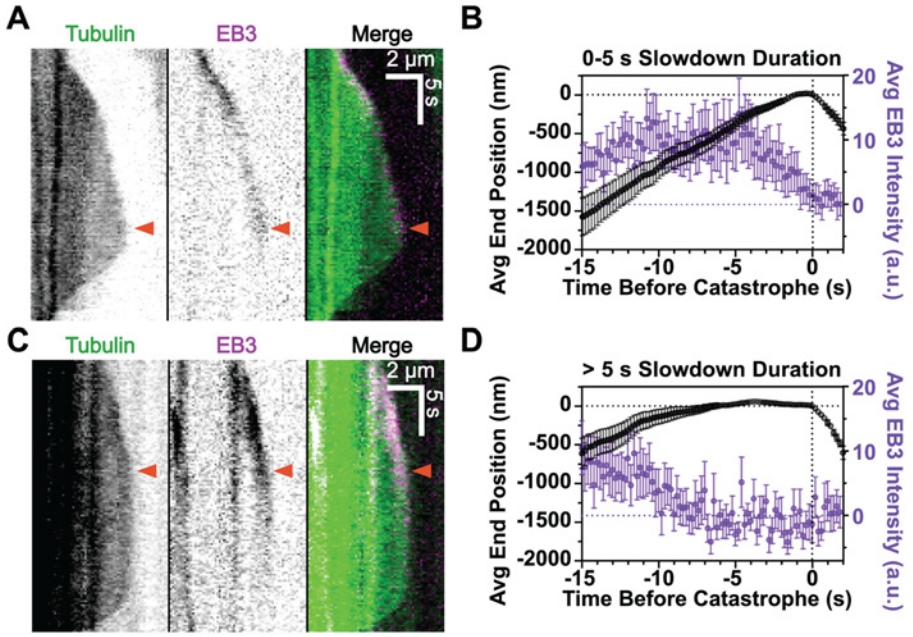

FIGURE 4: EB localization does not predict microtubule catastrophe in cells. LLC-PK1 cell stably expressing eGFP-α-Tubulin and transiently transfected with mCherry-EB3. (A) Example kymograph of a microtubule displaying a short slowdown duration (<5 s) prior to catastrophe. Arrowhead indicates onset of slowdown preceding catastrophe. (B) Average end position and EB3 intensity for events displaying up to a 5 s slowdown ($n = 15$ growth events). (C) Example kymograph of a microtubule displaying a long slowdown duration (>5 s) prior to catastrophe. Arrowhead indicates onset of slowdown preceding catastrophe. (D) Average end position and EB3 intensity for events displaying a slowdown >5 s ($n = 11$ growth events).

microtubule ends, in addition to imaging EB localization, we used fluorescent tubulin to determine the microtubule end position irrespective of its dynamic state. To collect two-color timelapses at sufficient temporal resolution, we turned to imaging LLC-PK1 cells stably expressing eGFP-α-tubulin (Rusan *et al.*, 2001) and transiently expressing mCherry-EB3 using spinning disk confocal (SDC) microscopy (Figure 4). EB1 and EB3 members of the EB protein family recognize the same nucleotide-dependent structure at growing microtubule ends. However, EB3 has been previously reported to display higher overall signal intensities while maintaining the same comet length as EB1 (Roth *et al.*, 2018). For this reason, we chose to introduce mCherry-EB3 into an established cell line stably expressing GFP-tubulin for simultaneous two-color imaging. Furthermore, although SDC does not provide super-resolution imaging, it allowed for fast time-lapse imaging (5 fps in two colors) with minimal photo damage over longer periods, which was necessary to fully capture a sufficient number of microtubule catastrophe events.

Our high-resolution analysis of catastrophe events in cells revealed that, similar to what has been previously observed in vitro, microtubule ends display a distinct slowdown period before the onset of catastrophe (Figure 4). However, in contrast to the in vitro conditions, where periods of slowdown prior to catastrophe are typically restricted to less than 5 s (Maurer *et al.*, 2014; Duellberg *et al.*, 2016; Farmer *et al.*, 2021; Mahserejian *et al.*, 2022), our data show that microtubule ends in cells can be maintained in a prolonged pre-catastrophe state. Indeed, detailed analysis of individual catastrophe events revealed a broad range of slowdown periods, with a mean duration of 7 ± 2 s (SEM, $n = 26$). The events displaying slowdown durations of less than 5 s were typically accompanied by the EB comet decay directly prior to catastrophe (Figure 4, A and B), as expected based on the previous observations in vitro (Maurer *et al.*, 2012, 2014; Duellberg *et al.*, 2016; Farmer *et al.*, 2021). Interestingly, a large fraction of the observed catastrophe events (11 out of 26 analyzed) displayed longer periods of slowdown lasting more than 5 s. For those events, EB end-localization was typically lost well before the onset of microtubule shrinkage (Figure 4, C and D). The finding that microtubule ends can resist depolymerization even after EB localization is lost demonstrates that EB comet loss is not a direct predictor of the immediate onset of microtubule catastrophe in cells.

Conclusions

In this study, we investigated the properties and function of the microtubule GTP-tubulin cap in cells. Using the same imaging modality and conditions, we found that microtubules polymerizing in interphase LLC-PK1 cells have the same EB comet sizes as microtubules grown at equivalent growth rates with purified proteins in vitro. Notably, our in vitro reconstitution assay employs only a limited set of proteins and does not capture the vast complexity of biochemical and biophysical conditions in cells. However, because these results were obtained through a direct comparison of cellular and in vitro microtubules, they validate the commonly used in vitro reconstitution assay as a faithful and relevant approach to study properties of the GTP-cap and mechanisms of microtubule dynamics in a minimal component system.

Microtubule dynamics and stability are regulated by myriad MAPs in cells. Given that the GTP-cap is considered to be the main stabilizing structure at growing microtubule ends (Kirschner and Mitchison, 1986; Hyman *et al.*, 1992; Caplow and Shanks, 1996; Duellberg *et al.*, 2016; Roostalu *et al.*, 2020; Farmer and Zanic, 2022), modulation of GTP-cap length presents a plausible

mechanism for regulation of microtubule stability by MAPs. Changing the size of the GTP-cap can be accomplished by changing either microtubule growth rate or GTP-hydrolysis rate. Several MAPs are known to directly modulate the microtubule growth rate (Akhmanova and Steinmetz, 2015; Gudimchuk and McIntosh, 2021; Lawrence *et al.*, 2023). Unless a MAP directly affects tubulin's GTP-hydrolysis rate, a MAP-driven change in microtubule growth rate will be accompanied by a corresponding change in the GTP-cap size, maintaining the consistent relationship between the two. Our finding that the relationship between the GTP-cap size and the microtubule growth rate is the same in cells as it is in a minimal in vitro system suggests that the rate of GTP-hydrolysis is not being differentially modulated in this cellular context.

The finding that the GTP-hydrolysis rate of tubulin is not regulated at growing microtubule ends in interphase cells, despite the complexity of regulatory MAPs present, is surprising. Several in vitro studies with purified proteins suggested that some MAPs may directly regulate the GTP-hydrolysis rate. Of note, a small reduction in the size of EB comets was reported at low, nonsaturating concentrations (1–10 nM) of EB proteins (Maurer *et al.*, 2012). Furthermore, recent cryo-EM studies reported that several MAPs recognize and/or promote particular conformations of tubulin dimers within the microtubule lattice that may be associated with different states in the tubulin GTP-hydrolysis cycle (Manka and Moores, 2018a). For example, high concentrations (~30 μM) of EB proteins induced a compacted and twisted structure of tubulin within microtubules grown with GTPγS, an analogue of GTP (Zhang *et al.*, 2015, 2018). Some MAPs, including tau and MAP2 were found to promote a compacted, GDP-like microtubule lattice (Kellogg *et al.*, 2018; Siahaan *et al.*, 2022), while others, like TPX2 and CAMSAP3, preferentially bind expanded microtubule lattices (Zhang *et al.*, 2017, 2018; Liu and Shima, 2023). Additionally, Kinesin-1 was shown to drive expansion of GDP-microtubule lattices (Peet *et al.*, 2018; Shima *et al.*, 2018; Verhey and Ohi, 2023). To what extent any of these tubulin conformations correspond to specific states in tubulin's GTP-hydrolysis cycle is largely unknown. In the case of EBs, recent studies using tubulin hydrolysis mutants concluded that EBs indeed recognize tubulin in a GTP-bound state and that the conformation of tubulin stabilized by EBs precedes GTP-hydrolysis (Geyer *et al.*, 2015; Roostalu *et al.*, 2020; LaFrance *et al.*, 2022). In this study, we used a well-established stably-expressing EB1-GFP LLC-PK1 cell line and found no aberrant effects on microtubule dynamics over the range of observed expression levels, consistent with previous characterizations of this cell line (Piehl and Cassimeris, 2003). Furthermore, under these conditions, we found no evidence for the modulation of the GTP-hydrolysis rate as the means to globally regulate cellular microtubule dynamics. It is possible that MAPs may directly modulate tubulin hydrolysis rate in a different cellular context, for example to achieve cell-cycle-dependent regulation of microtubule dynamics (Rusan *et al.*, 2001; Yamashita *et al.*, 2015). Alternatively, given that the exchangeable nucleotide in β-tubulin is readily accessible only at the exposed microtubule plus ends (Mitchison, 1993; Nogales *et al.*, 1998), direct regulation of the GTP-hydrolysis rate of tubulin within the microtubule may be difficult, and thus not a mechanism widely employed by MAPs. Investigation of these possibilities presents exciting directions for future research.

The idea that a bigger GTP-cap is generally more protective against microtubule catastrophe has been challenged by recent in vitro studies (Farmer and Zanic, 2022). Of note, microtubules polymerized in the presence of XMAP215 have accelerated growth rates and increased EB comet sizes, yet also display increased frequency of microtubule catastrophe (Farmer *et al.*, 2021). Furthermore, MAPs from the CLASP family do not change the microtubule growth rate or EB comet size, yet strongly suppress microtubule catastrophe (Lawrence *et al.*, 2018). Even in the absence of MAPs, slow-growing microtubule minus ends have small EB comets yet undergo significantly less frequent catastrophe when compared with their plus-end counterparts (Strothman *et al.*, 2019). In all these examples, the EB comet size reflects the corresponding microtubule growth rate. However, neither the mean growth rate nor the mean size of the EB comets can serve as an indicator of overall microtubule end stability (Farmer and Zanic, 2022).

Whether the protective GTP-cap is large or small, its removal and the transition from microtubule growth to rapid shrinkage likely involves an intermediate state of the microtubule end, characterized by a mixture of nucleotides and associated protofilament morphologies. Indeed, microtubule catastrophe has been characterized as a multi-step process (Odde *et al.*, 1995; Tran *et al.*, 1997; Gardner *et al.*, 2011, 2013; Lawrence *et al.*, 2023), and the onset of rapid microtubule shrinkage is typically preceded by a characteristic slowdown in microtubule growth rate (Maurer *et al.*, 2012; Farmer *et al.*, 2021; Mahserejian *et al.*, 2022). MAPs that induce uncoordinated protofilament polymerization and ragged microtubule end structures, such as XMAP215, promote fluctuations in microtubule growth that may ultimately drive microtubule catastrophe (Farmer *et al.*, 2021). Other MAPs, such as CLASPs, help microtubule ends resist catastrophe in spite of growth fluctuations, likely by stabilizing the pre-catastrophe intermediate and allowing the return of the end to a robustly growing state (Lawrence and Zanic, 2019; Aher *et al.*, 2020; Mahserejian *et al.*, 2022; Lawrence *et al.*, 2023). We find that microtubules in cells display large growth fluctuations, as well as notable growth slowdowns prior to catastrophe, during which the intensity of the EB comets is lost. Interestingly, however, the loss of EB comets in cells does not necessarily predict the onset of catastrophe. We speculate that this can be attributed to alternative mechanisms of microtubule end stabilization in cells, which do not rely on the presence of the GTP-cap. For example, anchoring of microtubule ends to the cell cortex or to other cellular structures can be achieved through a number of MAPs and motors, and thus prevent microtubule depolymerization (Gundersen, 2002; Laan *et al.*, 2012; Noordstra and Akhmanova, 2017; Seetharaman and Etienne-Manneville, 2019). Both binding of MAPs and post-translational modifications along the microtubule lattice are implicated in microtubule polymer stability (Verhey and Gaertig, 2007; Bodakuntla *et al.*, 2019; Janke and Magiera, 2020; Akhmanova and Kapitein, 2022)—how quickly these lattice-stabilizing mechanisms may be employed at dynamic microtubule ends in cells is an interesting question warranting future studies. From that perspective, rather than being the determinant of microtubule end stability, the role of the GTP-cap at the end of a growing microtubule may be to serve as a platform for the binding of myriad MAPs whose combinatorial effects ultimately decide the microtubule's fate.

MATERIALS AND METHODS

Protein preparation

Bovine brain tubulin was purified as previously described through cycles of polymerization and depolymerization in a high-molarity Pipes buffer (Castoldi and Popov, 2003). Tubulin was labeled with tetramethylrhodamine (TAMRA; Sigma-Aldrich) as described previously (Hyman, 1991). EB1-GFP was expressed and purified as

described previously (Zanic *et al.*, 2009) and stored in 10 mM BisTris, 10 mM Tris HCl, 100 mM KCl, 1 mM DTT, and 5% glycerol, pH 6.6. XMAP215 was expressed and purified as described previously (Farmer *et al.*, 2021) and stored in 10 mM Bis-Tris,10 mM Tris HCl, 100 mM KCl, 1 mM DTT, and 10% glycerol, pH 6.6. Protein concentration was determined using absorbance at $\lambda = 280$ nm.

In vitro assay conditions

Microtubules were imaged in chambers constructed as described previously (Gell *et al.*, 2010). In brief, three strips of Parafilm were sandwiched between 22 × 22 mm and 18 × 18 mm silanized coverslips to create two narrow channels for the exchange of reaction solutions. The channel surface was treated with 0.02 µg/µl anti-TAMRA antibody (Invitrogen) followed by 1% Pluronic F127 (Sigma-Aldrich) before use. GMPCPP-stabilized, 25% TAMRA-labeled microtubules were polymerized as described previously (Hunter *et al.*, 2003) and immobilized to coverslips using anti-TAMRA antibody (Gell *et al.*, 2010). A total of 12 µM tubulin, 200 nM EB1-GFP, and 100 nM XMAP215 were introduced into the chamber along with imaging buffer consisting of BRB80 supplemented with 40 mM D-glucose, 40 µg/ml glucose oxidase, 25 µg/ml catalase, 0.08 mg/ml casein, 10 mM DTT, 17 mM KCl and 0.1% methylcellulose.

Cell culture

LLC-PK1 EB1-GFP (pig kidney epithelial) cells were cultured in 1:1 DMEM and F12 media with 10% FBS and 1% PenStrep. LLC-PK1 EB1-GFP cells (originated from Piehl and Cassimeris, 2003) were a kind gift from Ryoma Ohi, University of Michigan. LLC-PK1 Tubulin-GFP cells were maintained in OptiMEM/Ham's-F-10 (1:1) media supplemented with 10% FBS and 1% PenStrep. LLC-PK1 Tubulin-GFP cells (originated from Rusan *et al.*, 2001) were a kind gift from Melissa Gardner, University of Minnesota. All cells were grown at 37°C with 5% CO_2. Prior to imaging the media was changed to FluoroBrite DMEM supplemented with 10% FBS.

Transfection

Approximately 24 h prior to transient transfection, LLC-PK1 Tubulin-GFP cells were split and seeded at ∼15% confluency in a 32 mm #1.5 precoated glass bottom dish. Cells were transiently transfected with 500 ng of mCherry-miniSOG-EB3-7, which was a gift from Michael Davidson (Addgene plasmid # 55089; http://n2t.net/addgene:55089; RRID:Addgene_55089) using Lipofectamine3000 at a 1:4 DNA to Lipofectamine ratio. Cells were incubated with plasmid and Lipofectamine3000 for ∼4 h at 37°C. After the 4-h incubation, the media was aspirated, and fresh media was added. Cells were imaged ∼20–24 h after transient transfection.

Determination of the effect of EB overexpression on microtubule dynamics

EB1-GFP overexpression levels were determined via corrected total cell fluorescence (CTCF) analysis. For the analysis, a freehand region of interest (ROI) was drawn around the cell area and in a region with no detectable signal (i.e., background) in FIJI ImageJ (Schindelin *et al.*, 2015; Rueden *et al.*, 2017). For each frame the ROI area, mean gray value, and the integrated density (average fluorescent intensity normalized to the ROI area) were measured. CTCF was then calculated using the following equation: CTCF = Integrated Density of cell ROI − (Area of cell ROI × Mean gray value of background ROI). CTCF for each frame was then averaged to determine the mean CTCF of the cell. To measure microtubule dynamics in each cell, Plustiptracker (Applegate *et al.*, 2011) was used. Prior to analyzing each video, the cell ROI that was drawn for the CTCF analysis was inverted and used to mask the background in the video to ensure that only EB comets within the cell of interest (with an associated CTCF) were tracked. Comets were detected using anisotropic Gaussian detection with an alpha value of 0.01 and a minimum distance between detected features of 5 to ensure that each comet was only detected once. For comet tracking, the *"microtubule plus-end dynamics"* tracking application was used. To prevent the chance of two tracks being linked incorrectly, both segment merging and segment splitting were deselected. For track analysis, the *"microtubule dynamics classification"* tracking application was used.

Imaging

Imaging was performed using either instant Structured Illumination Microscopy (iSIM) or SDC microscopy, as noted in the text. iSIM imaging was performed with a Visitech iSIM on a Nikon Ti2 stand using a Nikon SR HP Apo TIRF 100x/1.49-NA oil immersion objective at 1.5x zoom. Images were captured using a HamamatsuORCA-Fusion sCMOS camera. A Tokai Hit objective heater was used to maintain the sample at 35°C and with 5% CO_2. Images were acquired using BioVision imaging software. SDC imaging was performed on a Nikon Ti microscope with a Nikon SR HP Apo TIRF 100x/1.49-NA oil immersion objective. Images were captured with a Photometrics Prime 95B sCMOS camera using 488- and 561-nm solid-state lasers and standard filter sets using triggered two-color acquisition. A Tokai Hit objective heater was used to maintain the sample at 37°C and with 5% CO_2. Images were acquired using NIS-Elements (Nikon) software. SDC imaging was performed through use of the Vanderbilt Cell Imaging Shared Resource.

EB1 comet length analysis

EB1 comet lengths were determined using a series of custom MATLAB (vR2022b; MathWorks) scripts as reported previously (Farmer *et al.*, 2021). Briefly, the beginnings and ends of individual growth events were manually determined on kymographs and automatically divided into 5 s segments. The initial estimate of microtubule tip position over time was obtained assuming a constant growth rate between the first and last position. For each time frame, the pixel with the brightest EB1 intensity within a window (±5 pixels) around the initially estimated tip position was subsequently assigned as the microtubule tip position. The tip positions were then fitted by a linear regression to assign a growth rate to each 5 s segment. 5 s segments were then filtered to include only segments with well-defined growth rates using $R^2 > 0.8$ criterion. To generate time-averaged intensity profiles, the determined tip positions from each temporal frame within the 5 s segment were aligned. The microtubule lattice intensity was determined by averaging the intensity of 5 pixels and subsequently subtracted from the intensity of all pixels along the averaged intensity profile of a given segment. To determine EB1 comet length, the averaged intensity profiles were fitted to an exponential decay function using 25 pixels starting with the pixel immediately following the tip position (Bieling *et al.*, 2007; Farmer *et al.*, 2021): $I = Ae(-x/\lambda)$, where A is the intensity at pixel 1, and λ is the comet decay length. Exclusion of the 0th pixel intensity from the fit ensured that any potential subpixel perturbations in the tip structure not detected by our imaging did not affect the comet length measurement. Segments were then filtered to include only growth events where comet length could be confidently determined using $R^2 > 0.9$ criterion. Segments that met both R-squared criteria were then binned into

20 nm/s bins. As we were interested in comparing growth events in vitro and in cells over a shared growth rate range, data points outside of the shared data range were removed (83 in vitro growth events). Binned data was then subject to outlier analysis. Iterative Grubbs outlier analysis was then performed. As this outlier test requires at least seven data points, bins containing less than seven values were alternatively subjected to Grubbs outlier analysis. Following removal of outliers (no cell growth segments were removed in cells; five in vitro growth events were removed), any bins containing less than three values were removed (four cell growth events; seven in vitro growth events). Weighted averages and weighted error for each bin were then calculated using $1/CI^2$ weighting. The averaged data points were then fit to a linear regression with $1/Y^2$ weighting.

Determination of variability in microtubule growth

The EB1 channel was tracked with TipTracker_v3 (Demchouk *et al.*, 2011; Seetapun *et al.*, 2012; Prahl *et al.*, 2014) using MATLAB R2022a. Then, a custom MATLAB code was used to divide the output trajectories into continuous 10 s segments, allowing for gaps of no more than a total of 1 s within a given segment. The variations from the mean growth rate within the 10 s segments were quantified by performing the sum of squared residuals (SSR) analysis as described previously (Lawrence *et al.*, 2018; Farmer *et al.*, 2021). Briefly, using a custom MATLAB code, a linear function was fit to the length-versus-time data points to determine the mean growth rate. The SSR was calculated and normalized by the segment duration. For growth rate–matching experiments, only the trajectories with mean growth rates between 100 and 200 nm/s were considered. Outliers based on normalized SSR were identified using MATLAB function "isoutlier" and subsequently discarded. Unpaired Student's *t* test with Welch's correction was used to determine *P* values for mean velocity between experimental conditions, and a Mann–Whitney U test was used for normalized mean SSR.

Determination of the growth rate and EB intensity at the onset of catastrophe

To determine the EB3 intensity at the onset of catastrophe, we developed a custom MATLAB script based on previously published approaches (Maurer *et al.*, 2012; Duellberg *et al.*, 2016; Farmer *et al.*, 2021). To prepare videos for catastrophe analysis, ROIs around microtubules transitioning from growth to shrinkage during the 2-min acquisition period were cropped out. A kymograph of both tubulin and EB channels was produced from a line scan (width = 1) drawn along the microtubule of interest. This kymograph was used to determine if the microtubule underwent multiple catastrophes during the 2-min movie. If so, the video was temporally cropped so that only one catastrophe event occurred per a given movie. TipTracker_v3 (Demchouk *et al.*, 2011; Seetapun *et al.*, 2012; Prahl *et al.*, 2014) was used to determine the microtubule tip position from the tubulin channel. To increase the efficacy of tip tracking within the crowded cell, both the pad size (the number of pixels the code will search with respect to your input clicks) and line length for the Gaussian fit (the length of the line used to determine the tip position) were reduced; this led to a reduction in the number of tracking errors that arose as a result of encountering other microtubules and/or the cell edge. The *xy* coordinates for the microtubule tip position produced by TipTracker_v3 were assessed for accuracy by overlaying the output coordinates onto kymograph. If accurate, these coordinates were used in the MATLAB script to define the search coordinates for EB intensity.

Next, both *x* and *y* coordinates of the microtubule end from each temporal frame, except the initial and final frames, were preprocessed to eliminate tracking noise. If the difference between coordinates of the current frame and the previous frame was >220 nm (2x the pixel size), the current coordinate value was eliminated and a new coordinate value was interpolated using the previous and subsequent frame, assuming a linear growth rate (adapted from Rickman *et al.*, 2017; Farmer *et al.*, 2021). The "smoothdata" function in MATLAB was used with the "movmedian" method and a 10-frame (2 s) window size to further minimize tracking noise. The microtubule end position was determined using smoothened coordinates. To determine time of catastrophe, catastrophe was first approximated manually and then corrected using the following automated analysis: an instantaneous growth rate was determined for 15 frames before and after the manually approximated catastrophe time using a linear fit over a 3-frame sliding window. The linear fit was used to determine the moment in time 3 consecutive frames had velocity values greater than −50 nm/s, starting from 12 frames after catastrophe and moving backward in time. The latest of the three temporal frames of this moment was assigned as the automated, and final, time of catastrophe. The automated trajectories were manually inspected for accuracy by overlaying them onto the respective kymograph before further analysis.

A custom MATLAB code was used to determine the slowdown duration before catastrophe for each microtubule. Periods of slowdown were determined using two methods. 1) First, the velocity of a 5-frame segment ending at the time of catastrophe was determined by performing a linear fit, and the velocity value was assigned to all of the frames within this segment. Then, the segment size was increased frame by frame moving backward in time until the beginning of the growth event and the velocity of each segment was determined. If the velocity of a given segment was smaller than 50 nm/s, the frames in the given segment were marked as slowdowns. 2) The periods of slowdown were defined from velocities defined for 5-frame (1 s) segments of growth starting from the beginning of the growth event and moving toward the onset of catastrophe. If the velocity of a given segment was greater than 50 nm/s, the frames in that segment were marked as a regular growth event. This second pass allowed us to determine the beginning of a slowdown event with more accuracy. Then the duration of the slowdown was determined by finding the total number of frames that were marked as a slowdown by the running windows described above. We then separated microtubules into two groups: microtubules displaying either no or a short slowdown (i.e., 0–5 s, group 1) versus microtubules displaying long slowdowns (i.e., > 5 s, group 2).

The end positions of the growth events over time were aligned to generate an averaged microtubule tip position using a custom MATLAB code. For each microtubule, the time and position values were offset to assign the catastrophe event to (0,0). Subsequently, the mean and SEM of the positions at each timepoint were calculated for the two groups of microtubules based on their slowdown duration.

The EB3-mCherry intensity at microtubule ends preceding catastrophe was determined using a custom MATLAB function. Briefly, for each temporal frame in the video, the EB3-mCherry comet was rotated and centered around the microtubule end position (determined using the tubulin signal, as described above), such that the microtubule was horizontally aligned, and the EB3 comet was decaying to the right. The brightest intensity value within 5 lattice pixels and 1 solution pixel was assigned as the maximum EB3 intensity (5-pixel thickness, i.e., 5 × 6-pixel^2 area). Local

solution background intensity was determined by shifting the 5 × 6-pixel^2 area up and down by 7 pixels and calculating the mean intensity. Temporal frames with < 25 pixels available for background determination were discarded. For each temporal frame, the mean background intensity was then subtracted from the corresponding EB3 intensity. The average EB3 intensities as a function of time were obtained by averaging all growth events at every timepoint, with error being the SEM.

ACKNOWLEDGMENTS

We thank G. Brouhard (McGill University), R. Ohi (University of Michigan), and M. Gardner (University of Minnesota), for kindly gifting us the XMAP215 construct, LLC-PK1 EB1-GFP cells, and LLC-PK1 tubulin-GFP cells, respectively. We thank the Burnette laboratory (Vanderbilt University) for help with iSIM. All SDC microscopy imaging was performed through the use of the Vanderbilt Cell Imaging Shared Resource (supported by NIH grants CA68485, DK58404, and EY08126). Use of the core equipment was supported in part by Vanderbilt Ingram Cancer Center Resource Share Scholarship (2022-3739440). We thank the members of the Zanic laboratory for discussions and feedback. This work was supported by National Institutes of Health grant R35GM119552 to MZ. VF acknowledges support from National Institutes of Health grant T32GM008320 and American Heart Association Predoctoral Fellowship 19PRE34380083. AC acknowledges support from the National Institutes of Health grant T32GM008320. GA acknowledges support from Kadir Has University Startup Funds. The authors declare no competing financial interests.

REFERENCES

Aher A, Kok M, Sharma A, Rai A, Olieric N, Rodriguez-Garcia R, Katrukha EA, Weinert T, Olieric V, Kapitein LC, *et al.* (2018). CLASP suppresses microtubule catastrophes through a single TOG domain. Dev Cell 46, 40–58.e8.

Aher A, Rai D, Schaedel L, Gaillard J, John K, Liu Q, Altelaar M, Blanchoin L, Thery M, Akhmanova A (2020). CLASP mediates microtubule repair by restricting lattice damage and regulating tubulin incorporation. Curr Biol 30, 2175–2183.e6.

Akhmanova A, Kapitein LC (2022). Mechanisms of microtubule organization in differentiated animal cells. Nat Rev Mol Cell Biol 23, 541–558.

Akhmanova A, Steinmetz MO (2015). Control of microtubule organization and dynamics: Two ends in the limelight. Nat Rev Mol Cell Biol 16, 711–726.

Alberts B, Johnson A, Lewis J, Raff M, Roberts K, Walter P (2002). Molecular Biology of the Cell New York, USA: Garland Science.

Alushin GM, Lander GC, Kellogg EH, Zhang R, Baker D, Nogales E (2014). High-resolution microtubule structures reveal the structural transitions in $\alpha\beta$-tubulin upon GTP hydrolysis. Cell 157, 1117–1129.

Applegate KT, Besson S, Matov A, Bagonis MH, Jaqaman K, Danuser G (2011). plusTipTracker: Quantitative image analysis software for the measurement of microtubule dynamics. J Struct Biol 176, 168–184.

Bieling P, Laan L, Schek H, Munteanu EL, Sandblad L, Dogterom M, Brunner D, Surrey T (2007). Reconstitution of a microtubule plus-end tracking system in vitro. Nature 450, 1100–1105.

Bodakuntla S, Jijumon AS, Villablanca C, Gonzalez-Billault C, Janke C (2019). Microtubule-associated proteins: Structuring the cytoskeleton. Trends Cell Biol 29, 804–819.

Caplow M, Reid R (1985). Directed elongation model for microtubule GTP hydrolysis. Proc Natl Acad Sci USA 82, 3267–3271.

Caplow M, Shanks J (1996). Evidence that a single monolayer tubulin-GTP cap is both necessary and sufficient to stabilize microtubules. Mol Biol Cell 7, 663–675.

Carlier MF, Pantaloni D (1982). Assembly of microtubule protein: role of guanosine di- and triphosphate nucleotides. Biochemistry 21, 1215–1224.

Castoldi M, Popov AV (2003). Purification of brain tubulin through two cycles of polymerization-depolymerization in a high-molarity buffer. Protein Expr Purif 32, 83–88.

Coombes CE, Yamamoto A, Kenzie MR, Odde DJ, Gardner MK (2013). Evolving tip structures can explain age-dependent microtubule catastrophe. Curr Biol 23, 1342–1348.

Curd A, Cleasby A, Makowska K, York A, Shroff H, Peckham M (2015). Construction of an instant structured illumination microscope. Methods 88, 37–47.

Demchouk AO, Gardner MK, Odde DJ (2011). Microtubule tip tracking and tip structures at the nanometer scale using digital fluorescence microscopy. Cel Mol Bioeng 4, 192–204.

Dixit R, Barnett B, Lazarus JE, Tokito M, Goldman YE, Holzbaur ELF (2009). Microtubule plus-end tracking by CLIP-170 requires EB1. Proc Natl Acad Sci USA 106, 492–497.

Drechsel DN, Kirschner MW (1994). The minimum GTP cap required to stabilize microtubules. Curr Biol 4, 1053–1061.

Duellberg C, Cade NI, Holmes D, Surrey T (2016). The size of the EB cap determines instantaneous microtubule stability. Elife 5, e13470.

Estévez-Gallego J, Josa-Prado F, Ku S, Buey RM, Balaguer FA, Prota AE, Lucena-Agell D, Kamma-Lorger C, Yagi T, Iwamoto H, *et al.* (2020). Structural model for differential cap maturation at growing microtubule ends. Elife 9, e50155.

Farmer V, Arpağ G, Hall SL, Zanic M (2021). XMAP215 promotes microtubule catastrophe by disrupting the growing microtubule end. J Cell Biol 220, e202012144.

Farmer VJ, Zanic M (2023). Beyond the GTP-cap: Elucidating the molecular mechanisms of microtubule catastrophe. Bioessays 45, e2200081.

Gardner MK, Zanic M, Gell C, Bormuth V, Howard J (2011). Depolymerizing kinesins Kip3 and MCAK shape cellular microtubule architecture by differential control of catastrophe. Cell 147, 1092–1103.

Gardner MK, Zanic M, Howard J (2013). Microtubule catastrophe and rescue. Curr Opin Cell Biol 25, 14–22.

Gell C, Bormuth V, Brouhard GJ, Cohen DN, Diez S, Friel CT, Helenius J, Nitzsche B, Petzold H, Ribbe J, *et al.* (2010). Microtubule dynamics reconstituted in vitro and imaged by single-molecule fluorescence microscopy. Methods Cell Biol 95, 221–245.

Geyer EA, Burns A, Lalonde BA, Ye X, Piedra F-A, Huffaker TC, Rice LM (2015). A mutation uncouples the tubulin conformational and GTPase cycles, revealing allosteric control of microtubule dynamics. Elife 4, e10113.

Gudimchuk NB, McIntosh JR (2021). Regulation of microtubule dynamics, mechanics and function through the growing tip. Nat Rev Mol Cell Biol 22, 777–795.

Gundersen GG (2002). Evolutionary conservation of microtubule-capture mechanisms. Nat Rev Mol Cell Biol 3, 296–304.

Hiller G, Weber K (1978). Radioimmunoassay for tubulin: A quantitative comparison of the tubulin content of different established tissue culture cells and tissues. Cell 14, 795–804.

Hunter AW, Caplow M, Coy DL, Hancock WO, Diez S, Wordeman L, Howard J (2003). The kinesin-related protein MCAK is a microtubule depolymerase that forms an ATP-hydrolyzing complex at microtubule ends. Mol Cell 11, 445–457.

Hyman AA (1991). Preparation of marked microtubules for the assay of the polarity of microtubuie-based motors by fluorescence. J Cell Sci Suppl 14, 125–127.

Hyman AA, Salser S, Drechsel DN, Unwin N, Mitchison TJ (1992). Role of GTP hydrolysis in microtubule dynamics: Information from a slowly hydrolyzable analogue, GMPCPP. Mol Biol Cell 3, 1155–1167.

Janke C, Magiera MM (2020). The tubulin code and its role in controlling microtubule properties and functions. Nat Rev Mol Cell Biol 21, 307–326.

Juanes MA, Fees CP, Hoeprich GJ, Jaiswal R, Goode BL (2020). EB1 directly regulates APC-mediated actin nucleation. Curr Biol 30, 4763–4772.e8.

Kellogg EH, Hejab NMA, Poepsel S, Downing KH, DiMaio F, Nogales E (2018). Near-atomic model of microtubule-tau interactions. Science 360, 1242–1246.

Kirschner M, Mitchison T (1986). Beyond self-assembly: From microtubules to morphogenesis. Cell 45, 329–342.

Laan L, Roth S, Dogterom M (2012). End-on microtubule-dynein interactions and pulling-based positioning of microtubule organizing centers. Cell Cycle 11, 3750–3757.

LaFrance BJ, Roostalu J, Henkin G, Greber BJ, Zhang R, Normanno D, McCollum CO, Surrey T, Nogales E (2022). Structural transitions in the GTP cap visualized by cryo-electron microscopy of catalytically inactive microtubules. Proc Natl Acad Sci USA 119, e2114994119.

Lawrence EJ, Arpağ G, Norris SR, Zanic M (2018). Human CLASP2 specifically regulates microtubule catastrophe and rescue. Mol Biol Cell 29, 1168–1177.
Lawrence EJ, Chatterjee S, Zanic M (2023). CLASPs stabilize the pre-catastrophe intermediate state between microtubule growth and shrinkage. J Cell Biol 222, e202107027.
Lawrence EJ, Zanic M (2019). Rescuing microtubules from the brink of catastrophe: CLASPs lead the way. Curr Opin Cell Biol 56, 94–101.
Lawrence EJ, Zanic M, Rice LM (2020). CLASPs at a glance. J Cell Sci 133, jcs243097.
Liu H, Shima T (2023). Preference of CAMSAP3 for expanded microtubule lattice contributes to stabilization of the minus end. Life Sci Alliance 6, e202201714.
Mahserejian SM, Scripture JP, Mauro AJ, Lawrence EJ, Jonasson EM, Murray KS, Li J, Gardner M, Alber M, Zanic M, *et al*. (2022). Quantification of microtubule stutters: dynamic instability behaviors that are strongly associated with catastrophe. Mol Biol Cell 33, ar22.
Manka SW, Moores CA (2018a). Microtubule structure by cryo-EM: Snapshots of dynamic instability. Essays Biochem 62, 737–751.
Manka SW, Moores CA (2018b). The role of tubulin–tubulin lattice contacts in the mechanism of microtubule dynamic instability. Nat Struct Mol Biol 25, 607–615.
Maurer SP, Cade NI, Bohner G, Gustafsson N, Boutant E, Surrey T (2014). EB1 accelerates two conformational transitions important for microtubule maturation and dynamics. Curr Biol 24, 372–384.
Maurer SP, Fourniol FJ, Bohner G, Moores CA, Surrey T (2012). EBs recognize a nucleotide-dependent structural cap at growing microtubule ends. Cell 149, 371–382.
Mimori-Kiyosue Y, Shiina N, Tsukita S (2000). The dynamic behavior of the APC-binding protein EB1 on the distal ends of microtubules. Curr Biol 10, 865–868.
Mitchison T, Kirschner M (1984). Dynamic instability of microtubule growth. Nature 312, 237–242.
Mitchison TJ (1993). Localization of an exchangeable GTP binding site at the plus end of microtubules. Science 261, 1044–1047.
Nogales E, Downing KH, Amos LA, Löwe J (1998). Tubulin and FtsZ form a distinct family of GTPases. Nat Struct Mol Biol 5, 451–458.
Noordstra I, Akhmanova A (2017). Linking cortical microtubule attachment and exocytosis. F1000Res 6, 469.
Odde DJ, Cassimeris L, Buettner HM (1995). Kinetics of microtubule catastrophe assessed by probabilistic analysis. Biophys J 69, 796–802.
Peet DR, Burroughs NJ, Cross RA (2018). Kinesin expands and stabilizes the GDP-microtubule lattice. Nat Nanotechnol 13, 386–391.
Piehl M, Cassimeris L (2003). Organization and dynamics of growing microtubule plus ends during early mitosis. Mol Biol Cell 14, 916–925.
Prahl LS, Castle BT, Gardner MK, Odde DJ (2014). Quantitative analysis of microtubule self-assembly kinetics and tip structure. Methods Enzymol 540, 35–52.
Reid TA, Coombes C, Mukherjee S, Goldblum RR, White K, Parmar S, McClellan M, Zanic M, Courtemanche N, Gardner MK (2019). Structural state recognition facilitates tip tracking of EB1 at growing microtubule ends. Elife 8, e48117.
Rickman J, Duellberg C, Cade NI, Griffin LD, Surrey T (2017). Steady-state EB cap size fluctuations are determined by stochastic microtubule growth and maturation. Proc Natl Acad Sci 114, 3427–3432.
Roostalu J, Thomas C, Cade NI, Kunzelmann S, Taylor IA, Surrey T (2020). The speed of GTP hydrolysis determines GTP cap size and controls microtubule stability. Elife 9, e51992.
Roth D, Fitton BP, Chmel NP, Wasiluk N, Straube A (2018). Spatial positioning of EB family proteins at microtubule tips involves distinct nucleotide-dependent binding properties. J Cell Sci 132, jcs219550.
Roth S, Heintzmann R (2016). Optical photon reassignment with increased axial resolution by structured illumination. Methods Appl Fluoresc 4, 045005.
Rueden CT, Schindelin J, Hiner MC, DeZonia BE, Walter AE, Arena ET, Eliceiri KW (2017). ImageJ2: ImageJ for the next generation of scientific image data. BMC Bioinformatics 18, 529.
Rusan NM, Fagerstrom CJ, Yvon AM, Wadsworth P (2001). Cell cycle-dependent changes in microtubule dynamics in living cells expressing green fluorescent protein-alpha tubulin. Mol Biol Cell 12, 971–980.
Schindelin J, Rueden CT, Hiner MC, Eliceiri KW (2015). The ImageJ ecosystem: An open platform for biomedical image analysis. Mol Reprod Dev 82, 518–529.
Seetapun D, Castle BT, McIntyre AJ, Tran PT, Odde DJ (2012). Estimating the microtubule GTP cap size in vivo. Curr Biol 22, 1681–1687.
Seetharaman S, Etienne-Manneville S (2019). Microtubules at focal adhesions – a double-edged sword. J Cell Sci 132, jcs232843.
Shima T, Morikawa M, Kaneshiro J, Kambara T, Kamimura S, Yagi T, Iwamoto H, Uemura S, Shigematsu H, Shirouzu M, *et al*. (2018). Kinesin-binding–triggered conformation switching of microtubules contributes to polarized transport. J Cell Biol 217, 4164–4183.
Siahaan V, Tan R, Humhalova T, Libusova L, Lacey SE, Tan T, Dacy M, Ori-McKenney KM, McKenney RJ, Braun M, *et al*. (2022). Microtubule lattice spacing governs cohesive envelope formation of tau family proteins. Nat Chem Biol 18, 1224–1235.
Strothman C, Farmer V, Arpağ G, Rodgers N, Podolski M, Norris S, Ohi R, Zanic M (2019). Microtubule minus-end stability is dictated by the tubulin off-rate. J Cell Biol 218, 2841–2853.
Tirnauer JS, Grego S, Salmon ED, Mitchison TJ (2002). EB1–microtubule interactions in Xenopus egg extracts: Role of EB1 in microtubule stabilization and mechanisms of targeting to microtubules. Mol Biol Cell 13, 3614–3626.
Tournebize R, Popov A, Kinoshita K, Ashford AJ, Rybina S, Pozniakovsky A, Mayer TU, Walczak CE, Karsenti E, Hyman AA (2000). Control of microtubule dynamics by the antagonistic activities of XMAP215 and XKCM1 in Xenopus egg extracts. Nat Cell Biol 2, 13–19.
Tran PT, Walker RA, Salmon ED (1997). A Metastable intermediate state of microtubule dynamic instability that differs significantly between plus and minus ends. J Cell Biol 138, 105–117.
Urazbaev A, Serikbaeva A, Tvorogova A, Dusenbayev A, Kauanova S, Vorobjev I (2021). On the relationship between EB-3 profiles and microtubules growth in cultured cells. Front Mol Biosci 8, 745089.
Verhey KJ, Gaertig J (2007). The tubulin code. Cell Cycle 6, 2152–2160.
Verhey KJ, Ohi R (2023). Causes, costs and consequences of kinesin motors communicating through the microtubule lattice. J Cell Sci 136, jcs260735.
Yamashita N, Morita M, Legant WR, Chen B-C, Betzig E, Yokota H, Mimori-Kiyosue Y (2015). Three-dimensional tracking of plus-tips by lattice light-sheet microscopy permits the quantification of microtubule growth trajectories within the mitotic apparatus. J Biomed Opt 20, 101206.
York AG, Chandris P, Nogare DD, Head J, Wawrzusin P, Fischer RS, Chitnis A, Shroff H (2013). Instant super-resolution imaging in live cells and embryos via analog image processing. Nat Methods 10, 1122–1126.
Zanic M (2016). Measuring the effects of microtubule-associated proteins on microtubule dynamics In Vitro. In: The Mitotic Spindle: Methods and Protocols, ed. P Changand R Ohi, New York, NY: Springer, 47–61.
Zanic M, Stear JH, Hyman AA, Howard J (2009). EB1 recognizes the nucleotide state of tubulin in the microtubule lattice. PLoS One 4, e7585.
Zanic M, Widlund PO, Hyman AA, Howard J (2013). Synergy between XMAP215 and EB1 increases microtubule growth rates to physiological levels. Nat Cell Biol 15, 688–693.
Zhang R, Alushin GM, Brown A, Nogales E (2015). Mechanistic origin of microtubule dynamic instability and its modulation by EB proteins. Cell 162, 849–859.
Zhang R, LaFrance B, Nogales E (2018). Separating the effects of nucleotide and EB binding on microtubule structure. Proc Natl Acad Sci USA 115, E6191–E6200.
Zhang R, Roostalu J, Surrey T, Nogales E (2017). Structural insight into TPX2-stimulated microtubule assembly. Elife 6, e30959.